

Roughening Transition in a Moving Contact Line

Ramin Golestanian^{1,2,3} and Elie Raphaël¹

¹ *Laboratoire de Physique de la Matière Condensée, Collège de France, UMR 7125 et FR 2438 du CNRS, 11 place Marcelin-Berthelot, 75231 Paris Cedex 05, France*

² *Institute for Advanced Studies in Basic Sciences, Zanjan 45195-159, Iran*

³ *Institute for Studies in Theoretical Physics and Mathematics, P.O. Box 19395-5531, Tehran, Iran*
(November 12, 2018)

The dynamics of the deformations of a moving contact line on a disordered substrate is formulated, taking into account both local and hydrodynamic dissipation mechanisms. It is shown that both the coating transition in contact lines receding at relatively high velocities, and the pinning transition for slowly moving contact lines, can be understood in a unified framework as roughening transitions in the contact line. We propose a phase diagram for the system in which the phase boundaries corresponding to the coating transition and the pinning transition meet at a *junction* point, and suggest that for sufficiently strong disorder a receding contact line will leave a Landau–Levich film immediately after depinning. This effect may be relevant to a recent experimental observation in a liquid Helium contact line on a Cesium substrate [C. Guthmann, R. Gombrowicz, V. Repain, and E. Rolley, Phys. Rev. Lett. **80**, 2865 (1998)].

I. INTRODUCTION AND SUMMARY

When a drop of liquid spreads on a solid surface, the *contact line*, which is the common borderline between the solid, the liquid, and the corresponding equilibrium vapor, undergoes a rather complex dynamical behavior. This dynamics is determined by a subtle competition between the mutual interfacial energetics of the three phases, dissipation and hydrodynamic flows in the liquid, and the geometrical or chemical irregularities of the solid surface [1].

For a partially wetting fluid on sufficiently smooth substrates, a contact line at equilibrium has a well defined contact-angle θ_e that is determined by the solid-vapor γ_{SV} and the solid-liquid γ_{SL} interfacial energies, and the liquid surface tension γ through Young's relation: $\gamma_{SV} - \gamma_{SL} = \gamma \cos \theta_e$. For a moving contact line, however, the value of the so-called dynamic contact-angle θ changes as a function of velocity: $\theta > \theta_e$ for an advancing contact line and $\theta < \theta_e$ for a receding one. This is because the unbalanced interfacial force $\gamma_{SV} - \gamma_{SL} - \gamma \cos \theta$ now has to be balanced with a frictional force in a steady state situation. The dissipation in the moving contact line, which is responsible for the friction, can be either of *local* origin, for example due to microscopic jumps of single molecules (from the liquid into the vapor) in the immediate vicinity of the contact line [2,3], or due to viscous *hydrodynamic* losses inside the moving liquid wedge [1,4–7].

For a contact line that is receding at a velocity v , it has been shown by de Gennes [6] that a steady state is achieved in which the liquid will partially wet the plate with a nonvanishing dynamic contact-angle θ only for velocities less than a certain critical value. The dynamic contact-angle decreases with increasing v , until at the critical velocity the system undergoes a dynamical phase

transition in which a macroscopic Landau–Levich liquid film [8,9], formally corresponding to a vanishing θ , will remain on the plate. One can think of the dynamic contact-angle as the order parameter characterizing this *coating transition*, in analogy with equilibrium phase transitions, while velocity is playing the role of the tuning parameter. Elaborating further on this analogy then seems to suggest that the nature of the coating transition depends crucially on the dominant dissipation mechanism: In the local picture θ vanishes continuously as v approaches the critical velocity, which makes it look like a *second order* phase transition, while on the contrary, in the hydrodynamic picture a jump is predicted in θ from $\theta_e/\sqrt{3}$ to zero at the transition, which is the signature of a *first order* phase transition [6].

Another notable feature of contact lines, which is responsible for their novel dynamics, is their anomalous long-ranged elasticity [10]. For length scales below the capillary length (which is of the order of 3 mm for water at room temperature), a contact line deformation of wavevector k will distort the surface of the liquid over a distance $|k|^{-1}$. Assuming that the surface deforms instantaneously in response to the contact line, the elastic energy cost for the deformation can be calculated from the surface tension energy stored in the distorted area, and is thus proportional to $|k|$. The anomalous elasticity leads to interesting equilibrium dynamics, corresponding to when the contact line is perturbed from its static position, as studied by de Gennes [11]. Balancing the rate of interfacial energy change and the dissipation, which he assumed for small contact-angles is dominated by the hydrodynamic dissipation in the liquid nearby the contact line, he finds that each deformation mode relaxes to equilibrium with a characteristic (inverse) decay time $\tau^{-1}(k) = c|k|$, where c is a characteristic *relaxation velocity* [11]. The relaxation is thus characterized by a dy-

dynamic exponent z , defined via $\tau^{-1}(k) \sim |k|^z$, which is equal to 1. The linear dispersion relation implies that a deformation in the contact line will *decay* and *propagate* at a constant velocity, as opposed to systems with normal line tension elasticity, where the decay and the propagation are governed by diffusion. This behavior has been observed, and the linear dispersion relation has been precisely tested, in a recent experiment by Ondarcuhu and Veyssie [12].

In reality, the presence of defects and heterogeneities in the substrate, which could be due to (surface) roughness or chemical contamination, further complicates the dynamics of a contact line [13,14]. In the presence of such heterogeneities, a contact line at equilibrium becomes *rough*, because it tries to locally deform so as to find the path with optimal *pinning* energy [1]. This is in contrast to the case of a perfect solid surface, where the contact line is *flat*. The roughness can be characterized as a scaling law that relates the statistical width W of the contact line to its length L , via $W \sim L^\zeta$. The so-called roughness exponent ζ is equal to 1/3 for a contact line at equilibrium on a surface with short-range correlated disorder [15–18]. Since the contact line is pinned by the defects, a nonzero (critical) force is necessary to set it to motion, through a *depinning* transition [19–22]. For a contact line at the depinning threshold, a roughness exponent about 0.4 has been predicted theoretically from two-loop field theoretical renormalization group calculations [23], and numerical simulations [24], which seems to disagree with the experimental finding of 0.5 for both liquid Helium on a Cesium substrate [25] and water on glass experiments [26]. It is also important to note that there may be numerous metastable states for the contact line due to the random disorder, leading to hysteresis in the contact-angle [10,16].

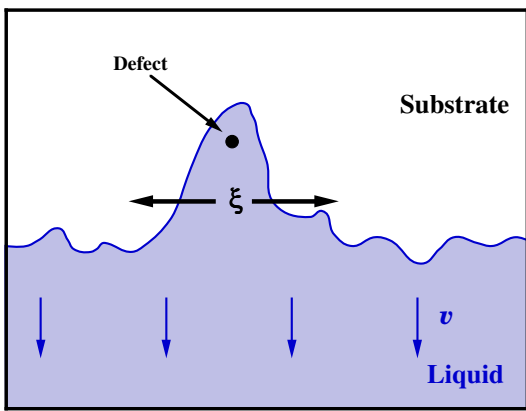


FIG. 1. A contact line moving on a disordered substrate undergoes shape fluctuations. A portion of the contact line can be instantaneously pinned by a defect, thereby nucleating domains of typical sizes given by a correlation length ξ . These domains become rough, because they have to conform to the minimum energy configuration on the substrate. At the onset of a roughening transition this correlation length diverges.

Here we study the *nonequilibrium* dynamics of the deformations of a moving contact line on a disordered substrate [27,28]. The dynamics is governed by a balance between three different forces: (i) the interfacial force, (ii) the frictional force which can stem from either local or hydrodynamic dissipation processes, and (iii) a random force caused by the disorder. We find that the relaxation spectrum of a moving contact line is the same as the equilibrium case, but the characteristic relaxation velocity depends on v : It decreases with v until at the critical velocity corresponding to the coating transition it vanishes identically. The progressively slow relaxation of a distorted contact line near the coating transition is in agreement with a nucleation picture of the phase transition (See Fig. 1).

We find that coating transition can be actually understood in terms of a *roughening transition* of the contact line on the disordered substrate. Since linear relaxation becomes infinitely slow in the vicinity of the coating transition, the dominant relaxation is thus governed by non-linear terms in the dynamical equation, and the dynamical phase transition can thus be properly accounted for only by using systematic renormalization group (RG) calculations. We find that disorder favors the coating transition, in the sense that the onset of leaving a Landau–Levich film for a random substrate with strength g takes place at a dynamic contact-angle

$$\left. \frac{\theta_c}{\theta_e} \right|_l = \alpha_{cl} \left(\frac{g}{\gamma \theta_e^2} \right)^{1/3}, \quad (1)$$

for local dissipation, and

$$\left. \frac{\theta_c}{\theta_e} \right|_h = \frac{1}{\sqrt{3}} + \alpha_{ch} \left(\frac{g}{\gamma \theta_e^2} \right)^{2/3}, \quad (2)$$

for hydrodynamic dissipation, to the leading order. (α_{cl} and α_{ch} are numerical constants to be defined below.) The value of the roughness exponent at the transition is found to determine the order of the transition. Although we find that this exponent acquires non-universal values, it appears that the predicted nature of the phase transition from the RG calculation is in agreement with the mean-field results, i.e. second order for local case and first order for hydrodynamic case, for sufficiently weak disorder.

For a sufficiently slowly moving contact line, we find that a *pinning transition* takes place, which is the reverse of the depinning transition, and that it can also be understood as a roughening transition. We obtain the phase boundary for this transition corresponding to the advancing and receding contact angles at the onset of pinning as

$$\left. \frac{\theta_a^2}{\theta_e^2} \right|_l - 1 = 1 - \left. \frac{\theta_r^2}{\theta_e^2} \right|_l = \alpha_{pl} \left(\frac{g}{\gamma \theta_e^2} \right)^2, \quad (3)$$

for the local case, and

$$\left. \frac{\theta_a^2}{\theta_e^2} \right|_h - 1 = 1 - \left. \frac{\theta_r^2}{\theta_e^2} \right|_h = \alpha_{ph} \left(\frac{g}{\gamma \theta_e^2} \right)^2, \quad (4)$$

for the hydrodynamic case, to the leading order, which is in agreement with a previous prediction by Robbins and Joanny [16]. (α_{pl} and α_{ph} are numerical constants to be defined below.) We further find that the roughness exponent at the pinning threshold is also non-universal.

We combine our results for the coating transition and the pinning transition, and propose a phase diagram for contact lines with local dissipation as depicted in Fig. 2, and a corresponding one for contact lines with hydrodynamic dissipation as depicted in Fig. 3. In particular, we find that the phase boundaries corresponding to the coating transition and the pinning transition meet at a junction point T , and suggest that for sufficiently strong disorder a receding contact line will leave a Landau–Levich film immediately after depinning. This corresponds to the dashed lines in Figs. 2 and 3. Note that the asymptotic form for the coating transition lines in Figs. 2 and 3 are given in Eqs. (1) and (2), and the asymptotic form for the pinning transition lines are given in Eqs. (3) and (4), respectively.

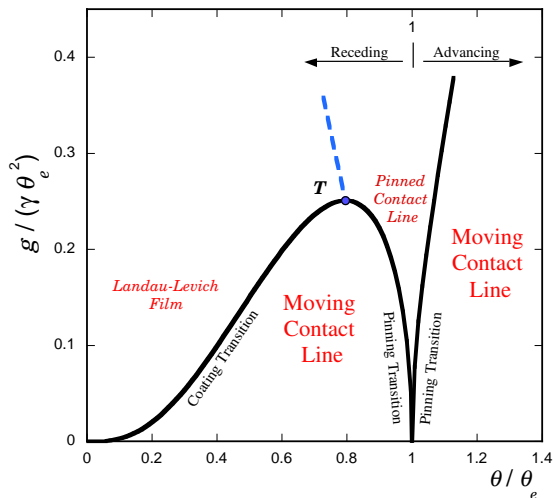


FIG. 2. The suggested phase diagram of a contact line with *local* dissipation on a disordered substrate. The asymptotic forms for the coating and pinning transition lines are given in Eqs. (1) and (3), respectively.

The rest of this article is organized as follows. In Sec. II, the main ingredients in the dynamics of the contact line are discussed, and they are put together in Sec. III where a stochastic dynamical equation is proposed. In Sec. IV, the stochastic dynamical equation is characterized by its self-affine behavior in terms of various exponents. The mean-field theory of a moving contact line is discussed in Sec. V, accompanied by a linear relaxation theory in Sec. VI. The effect of the nonlinearities is incorporated using a dynamical RG scheme which is discussed in Sec. VII, followed by the results in Sec. VIII

and some discussions in Sec. IX. Some details related to the differential geometry of the moving liquid drop is relegated to Appendix A, and finally some useful asymptotic forms of the results presented in Sec. III are given in Appendix B.

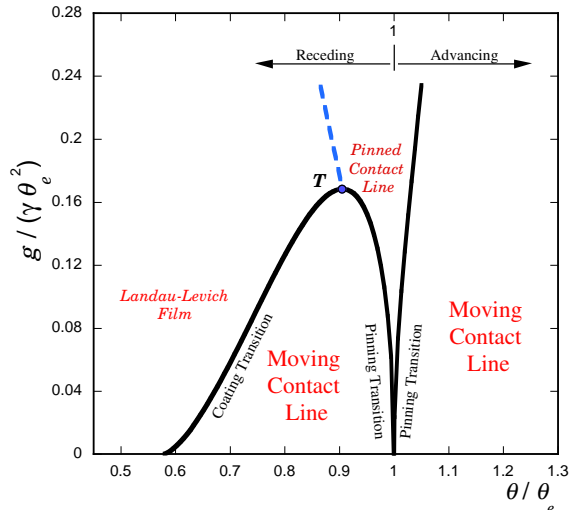


FIG. 3. The suggested phase diagram of a contact line with *hydrodynamic* dissipation on a disordered substrate. The asymptotic forms for the coating and pinning transition lines are given in Eqs. (2) and (4), respectively. Note that the coating transition line starts at $1/\sqrt{3} \simeq 0.577$ for zero disorder.

II. DYNAMICS OF A DEFORMING CONTACT LINE

Let us assume that the contact line is oriented along the x -axis, and is moving in the y -direction with the position described by $y(x, t) = vt + h(x, t)$, as depicted in Fig. 4.

A. Interfacial Forces

If a line element of length $dl = dx\sqrt{1 + (\partial_x h)^2}$ is displaced by $\delta y(x, t)$, the interfacial energy will be locally modified by two contributions: (i) the difference between the solid-vapor γ_{SV} and the solid-liquid γ_{SL} interfacial energies times the swept area in which liquid is replaced by vapor, namely, $(\gamma_{SV} - \gamma_{SL})dl\delta y/\sqrt{1 + (\partial_x h)^2}$, and (ii) the work done by the surface tension force, whose direction is along the unit vector $\hat{\mathbf{T}}$ that is parallel to the liquid-vapor interface at the contact and perpendicular to the contact line, as $\gamma\hat{\mathbf{T}} \cdot \hat{\mathbf{y}}dl\delta y$. Note that we are interested in length scales below the capillary length, where gravity does not play a role. The overall change in the interfacial energy of the system can thus be written as

$$\delta E = \int dx \sqrt{1 + (\partial_x h)^2} \left[\frac{\gamma \cos \theta_e}{\sqrt{1 + (\partial_x h)^2}} - \gamma \hat{\mathbf{T}} \cdot \hat{\mathbf{y}} \right] \delta y(x, t), \quad (5)$$

in which we have made use of the Young equation. Note that both “forces” should be projected onto the y -axis when calculating the work done for a displacement in this direction.

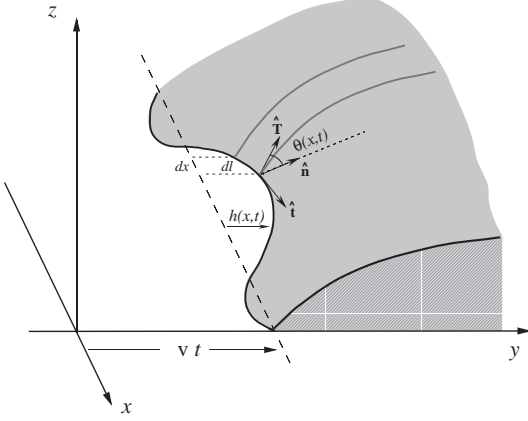


FIG. 4. The schematics of the system.

B. Dissipation

To calculate the dissipation relevant to the dynamics of the contact line, we should consider only the *normal* component of the velocity [3]. If the contact-angle is very small, the dominant contribution to the dissipation comes from the viscous losses in the hydrodynamic flows of the liquid wedge [1]. For a slightly deformed contact line, we can assume that the dissipation is well approximated by the sum of contributions from wedge-shaped slices with local contact-angles $\theta(x, t)$, as shown in Fig. 4. This is a reasonable approximation because most of the dissipation is taking place in the singular flows near the tip of the wedge [1,11]. Using the result for the dissipation in a perfect wedge which is based on the lubrication approximation [1,29], we can calculate the dissipation in the hydrodynamic regime as

$$P_h = \frac{1}{2} \int dx \sqrt{1 + (\partial_x h)^2} \left(\frac{3\eta\ell}{\theta(x, t)} \right) \left[\frac{v + \partial_t h(x, t)}{\sqrt{1 + (\partial_x h)^2}} \right]^2, \quad (6)$$

where η is the viscosity of the liquid and ℓ is a logarithmic factor of order unity [11]. One can show that the error in the above estimate, which comes from overlap between the neighboring slices, only leads to curvature terms that are sub-dominant in the long wavelength limit.

Another physical process that is involved in causing dissipation is molecular jumps near the tip of the contact line, and is local in nature [2]. Therefore, in any

small neighborhood the amount of dissipation is completely determined by the local value of the contact line velocity, while all the molecular details of the dissipation is encoded in an effective friction coefficient μ^{-1} . The overall dissipation can then be written as

$$P_l = \frac{1}{2\mu} \int dx \sqrt{1 + (\partial_x h)^2} \left[\frac{v + \partial_t h(x, t)}{\sqrt{1 + (\partial_x h)^2}} \right]^2. \quad (7)$$

C. Force Balance

We can find the governing dynamical equation by balancing the total friction force obtained as $\delta(P_l + P_h)/\delta\partial_t h(x, t)$ with the interfacial force $-\delta E/\delta h(x, t)$ at each point along the contact line. In the limit of small contact-angles, we find [30]

$$\left[\frac{1}{\mu} + \frac{3\eta\ell}{\theta(x, t)} \right] \frac{v + \partial_t h(x, t)}{\sqrt{1 + (\partial_x h)^2}} = \frac{\gamma}{2} [\theta_e^2 - \theta(x, t)^2]. \quad (8)$$

The above equation might simply be recovered by locally applying the result of Ref. [31] for straight contact lines, with the additional geometrical factor (that is needed when the direction of motion is not perpendicular to the contact line [3]) taken into account.

We can introduce a characteristic velocity for the hydrodynamic friction as $c_{0h} = \gamma\theta_e^3/(3\eta\ell)$, and a corresponding velocity for the local friction as $c_{0l} = \mu\gamma\theta_e^2$. It is then useful to write the dynamical force balance equation in terms of these characteristic velocities. It reads

$$\left[\frac{1}{c_{0l}} + \frac{1}{c_{0h}} \frac{\theta_e}{\theta(x, t)} \right] \frac{v + \partial_t h(x, t)}{\sqrt{1 + (\partial_x h)^2}} = \frac{1}{2} \left[1 - \frac{\theta(x, t)^2}{\theta_e^2} \right]. \quad (9)$$

Note that the relative strength of the two dissipation mechanisms is characterized by the ratio c_{0h}/c_{0l} , and we can readily obtain the asymptotic form of the equation when local dissipation is dominant by taking the limit $c_{0h}/c_{0l} \rightarrow \infty$, and the corresponding form when hydrodynamic dissipation dominates by taking the limit $c_{0h}/c_{0l} \rightarrow 0$.

D. Solving for the Surface Profile

To complete the calculation, we need to solve for the profile of the surface, and in particular, the angle $\theta(x, t)$ as a function of $h(x, t)$.

We may assume that the pressure at the surface equilibrates rapidly enough, so that for the effective study of the long time dynamics of the contact line it will be sufficient to set the instantaneous Laplace pressure to zero [10,11]. For sufficiently small contact-angles, the surface

profile $z(x, y, t)$ near the contact line can then be found as a solution of the Laplace equation

$$\nabla^2 z(x, y, t) = 0. \quad (10)$$

One can write a general solution for Eq. (10), of the form

$$z(x, y, t) = \theta(y - vt) + \int \frac{dk}{2\pi} \beta(k, t) \exp[ikx - |k|(y - vt)], \quad (11)$$

that yields the moving liquid wedge profile for a flat contact line. Imposing the boundary condition $z(x, vt + h(x, t), t) = 0$ at the position of the contact line then yields

$$\beta(k, t) = -\theta \left[h(k, t) + \int \frac{dq}{2\pi} |q| h(q, t) h(k - q, t) + O(h^3) \right]. \quad (12)$$

Note that we have performed the calculation up to the second order in h to find the leading order nonlinearity in the dynamical equation, and that since the nonlinear terms neglected in the expression for Laplace pressure are of the third order in z , this calculation is consistent.

From the slope of the liquid surface at the position of the contact line (see Fig. 4 and Appendix A) one can then obtain an expression for the contact-angle as a function of the contact line deformation. We find

$$\begin{aligned} \theta(x, t) = \theta \left\{ 1 + b_0 \int \frac{dk}{2\pi} |k| h(k, t) e^{ikx} \right. \\ \left. + \frac{1}{2} \int \frac{dk}{2\pi} \frac{dk'}{2\pi} [b_1 k k' + b_2 |k| |k'| \right. \\ \left. + b_3 |k + k'| (|k| + |k'| - |k + k'|)] \right. \\ \left. \times h(k, t) h(k', t) e^{i(k+k')x} \right\}, \quad (13) \end{aligned}$$

with $b_0 = 1$, $b_1 = 1$, $b_2 = 0$, and $b_3 = 1$. This can then be used in Eq. (8) to yield the dynamical equation.

One may, however, question the validity of the instantaneous pressure relaxation assumption. To improve on this approximation, one should attempt to solve for the dynamics of the liquid surface together with the contact line dynamics, and examine the corresponding time scales for the surface and contact line relaxations.

This dynamics can be formulated, within the framework of the lubrication approximation, using a continuity equation of the form

$$\partial_t z(x, y, t) = \nabla \cdot \left(\frac{z^3}{3\eta} \nabla p \right), \quad (14)$$

where the fluid film is locally described as a Poiseuille flow under the influence of the gradient of the Laplace pressure

$$p(x, y, t) = -\gamma \nabla^2 z(x, y, t). \quad (15)$$

Combining the above equations then yields

$$\partial_t z(x, y, t) + \frac{\gamma}{3\eta} \nabla \cdot [z^3 \nabla \nabla^2 z] = 0, \quad (16)$$

which is the dynamical equation for the surface deformation in the lubrication approximation [9]. To proceed systematically, one should attempt to solve Eq. (16) for a moving contact line with equilibrium contact-angle θ_e subject to the boundary condition $z(x, vt + h(x, t), t) = 0$, perturbatively in powers of the contact line deformation h up to second order. Unfortunately, this seems to be a formidable task, because of the complex structure of this nonlinear partial differential equation. In fact even at the zeroth order, i.e. for the case of a flat contact line, this problem is still the subject of much theoretical investigation [1,4,6,29,32].

We can instead try to estimate the surface relaxation time from Eq. (16) using dimensional arguments. If we consider a deformation of the characteristic size q^{-1} (in both x and y directions), and put in a wedge-like profile in the nonlinear term of Eq. (16) of the form $z \sim \theta q^{-1}$, we find that the corresponding (inverse) relaxation time scales as $\tau^{-1}(q) \sim (\gamma \theta^3 / \eta) q$. Interestingly, this is the same as the time scale that we find for the contact line relaxation [see Eq. (48) below], and it shows that the instantaneous surface relaxation assumption is not feasible. However, since surface relaxation introduces no new time or length scales in the system, it seems plausible to assume that the contact-angle profile as a function of the contact line deformation, as obtained from a full systematic solution of Eq. (16), will still maintain the form given in Eq. (13) in the long time and long length-scale limit, perhaps with different values for the numerical coefficients b_n . Since we will be interested only in this limit in the context of the RG calculations, it seems reasonable to use the general form proposed in Eq. (13).

E. Disorder

In most practical cases, the dynamics of a contact line is affected by the defects and heterogeneities in the substrate, in addition to dissipation and elasticity that we have considered so far. If the interfacial energies γ_{SV} and γ_{SL} are space dependent with the corresponding averages being $\bar{\gamma}_{SV}$ and $\bar{\gamma}_{SL}$, a displacement $\delta y(x, t)$ of the contact line is going to lead to a change in energy as

$$\delta E_d = \int dx g(x, vt + h(x, t)) \delta y(x, t), \quad (17)$$

where

$$g(x, y) = \gamma_{SV}(x, y) - \gamma_{SL}(x, y) - (\bar{\gamma}_{SV} - \bar{\gamma}_{SL}). \quad (18)$$

Incorporating this contribution in the force balance leads to an extra force term $g(x, vt)$ on the right hand side of

Eq.(8), which would act as a noise term in the dynamical equation for contact line deformation of the form

$$\eta(x, t) = \left(\frac{\mu\theta}{\theta + 3\eta\mu\ell} \right) g(x, vt), \quad (19)$$

to the leading order.

Assuming that the surface disorder has short range correlations (so that the correlation length is a microscopic length a) with a strength g , with a Gaussian distribution described by

$$\begin{aligned} \langle g(x, y) \rangle &= 0, \\ \langle g(x, y)g(x', y') \rangle &= g^2 a^2 \delta(x - x') \delta(y - y'), \end{aligned} \quad (20)$$

we can deduce the distribution of the noise as

$$\begin{aligned} \langle \eta(x, t) \rangle &= 0, \\ \langle \eta(x, t)\eta(x', t') \rangle &= 2D\delta(x - x')\delta(t - t'), \end{aligned} \quad (21)$$

where the strength of the noise is given as

$$D = \frac{g^2 a^2}{2|v|} \left(\frac{\mu\theta}{\theta + 3\eta\mu\ell} \right)^2. \quad (22)$$

III. DYNAMICAL EQUATION OF MOTION

We can now put together all the different ingredients of the dynamics of the contact line that we discussed in Sec. II, and obtain the governing dynamical equation. Inserting Eq. (13) in the force balance relation Eq. (9), and adding the noise term of Eq. (19), we find

$$\begin{aligned} \partial_t h(k, t) &= -c|k|h(k, t) + \eta(k, t) \\ &\quad - \frac{1}{2} \int \frac{dq}{2\pi} \lambda(q, k - q) h(q, t) h(k - q, t), \end{aligned} \quad (23)$$

up to the second order in deformations, with a corresponding nonlinear coupling as

$$\begin{aligned} \lambda(q, k - q) &= -\lambda_1 q(k - q) + \lambda_2 |q||k - q| \\ &\quad + \lambda_3 |k|(|q| + |k - q| - |k|). \end{aligned} \quad (24)$$

The zeroth order term in the force balance equation provides the contact-angle–velocity relation as

$$v = \frac{c_{0h}}{2} \frac{\theta}{\theta_e} \left[\frac{1 - \frac{\theta^2}{\theta_e^2}}{1 + \frac{c_{0h}}{c_{0l}} \frac{\theta}{\theta_e}} \right], \quad (25)$$

and we can also find the other coupling constants, namely the relaxation speed

$$c = \frac{c_{0h}}{2} \frac{\theta}{\theta_e} \left[\frac{\left(3 \frac{\theta^2}{\theta_e^2} - 1 + 2 \frac{c_{0h}}{c_{0l}} \frac{\theta^3}{\theta_e^3} \right)}{\left(1 + \frac{c_{0h}}{c_{0l}} \frac{\theta}{\theta_e} \right)^2} b_0 \right], \quad (26)$$

and the nonlinear coupling constants

$$\lambda_1 = \frac{c_{0h}}{2} \frac{\theta}{\theta_e} \left[\frac{\left(\frac{\theta^2}{\theta_e^2} - 1 \right)}{\left(1 + \frac{c_{0h}}{c_{0l}} \frac{\theta}{\theta_e} \right)} + \frac{\left(1 - 3 \frac{\theta^2}{\theta_e^2} - 2 \frac{c_{0h}}{c_{0l}} \frac{\theta^3}{\theta_e^3} \right)}{\left(1 + \frac{c_{0h}}{c_{0l}} \frac{\theta}{\theta_e} \right)^2} b_1 \right], \quad (27)$$

and

$$\begin{aligned} \lambda_2 &= \frac{c_{0h}}{2} \frac{\theta}{\theta_e} \left[\frac{\left(3 \frac{\theta^2}{\theta_e^2} - 1 + 2 \frac{c_{0h}}{c_{0l}} \frac{\theta^3}{\theta_e^3} \right)}{\left(1 + \frac{c_{0h}}{c_{0l}} \frac{\theta}{\theta_e} \right)^2} b_2 \right. \\ &\quad \left. + \frac{\left(3 \frac{\theta^2}{\theta_e^2} + \frac{c_{0h}}{c_{0l}} \frac{\theta}{\theta_e} + 3 \frac{c_{0h}}{c_{0l}} \frac{\theta^3}{\theta_e^3} + \frac{c_{0h}^2}{c_{0l}^2} \frac{\theta^4}{\theta_e^4} \right)}{\left(1 + \frac{c_{0h}}{c_{0l}} \frac{\theta}{\theta_e} \right)^3} (2b_0^2) \right], \end{aligned} \quad (28)$$

and

$$\lambda_3 = \frac{c_{0h}}{2} \frac{\theta}{\theta_e} \left[\frac{\left(3 \frac{\theta^2}{\theta_e^2} - 1 + 2 \frac{c_{0h}}{c_{0l}} \frac{\theta^3}{\theta_e^3} \right)}{\left(1 + \frac{c_{0h}}{c_{0l}} \frac{\theta}{\theta_e} \right)^2} b_3 \right], \quad (29)$$

in terms of the dynamic contact-angle. The spectrum of the noise term in Fourier space is characterized as

$$\begin{aligned} \langle \eta(k, t) \rangle &= 0, \\ \langle \eta(k, t)\eta(k', t') \rangle &= 2D(2\pi)\delta(k + k')\delta(t - t'), \end{aligned} \quad (30)$$

where the strength of the noise D is given as in Eq. (22), or equivalently as

$$D = \frac{a^2}{\left| 1 - \frac{\theta^2}{\theta_e^2} \right|} \frac{\left(c_{0h} \frac{\theta}{\theta_e} \right)}{\left(1 + \frac{c_{0h}}{c_{0l}} \frac{\theta}{\theta_e} \right)} \left(\frac{g}{\gamma\theta_e^2} \right)^2. \quad (31)$$

The above dynamical equation and its corresponding physical implications will be discussed in detail in the following sections. Since we will be attempting to compare the two alternative dissipation scenarios during these discussions, we have summarized in Appendix B the limiting form of the above equations corresponding to each of these mechanisms separately.

IV. CHARACTERIZING THE STOCHASTIC DYNAMICS

Due to the presence of the heterogeneities in the substrate, the contact line undergoes dynamical fluctuations during its (average) drift motion. These fluctuations, which are governed by the stochastic dynamical equation given in Sec. III [Eq. (23)], can best be characterized by the width of the contact line, which is defined as

$$W^2(L, t) \equiv \frac{1}{L^d} \int d^d \mathbf{x} \langle h(\mathbf{x}, t)^2 \rangle = \int \frac{d^d \mathbf{k}}{(2\pi)^d} \langle |h(\mathbf{k}, t)|^2 \rangle, \quad (32)$$

where the averaging is with respect to the noise term in Eq. (23). Note that we have generalized the contact line to a d -dimensional object of size L so that the dependence on the dimensionality becomes manifest.

Since the stochastic dynamics described by Eq. (23) corresponds to scale-free fluctuations, the resulting two-point correlation function should have a scaling form as

$$\langle |h(\mathbf{k}, t)|^2 \rangle = \frac{1}{k^{d+2\zeta}} \mathcal{G}(k^z t). \quad (33)$$

The function $\mathcal{G}(u)$ has the property that it saturates to a finite value for large u , to ensure that a stationary regime can be achieved in the long time limit. Using the above scaling form, the width of the contact line will be given as

$$W^2(L, t) \sim \int_{\pi/L}^{\pi/a} \frac{dk}{k^{1+2\zeta}} \mathcal{G}(k^z t), \quad (34)$$

that yields

$$W(L, t) \sim \begin{cases} t^{\zeta/z} & ; t \ll L^z \\ L^\zeta & ; t \gg L^z \end{cases}. \quad (35)$$

From equilibrium phase transitions, say in a magnetic system, we know that the fluctuations in the overall magnetization is proportional to the susceptibility, which is a response function. It is known that this quantity diverges at the critical point for second order phase transitions, while it stays finite for first order phase transitions. For a d -dimensional system of size L , the divergence appears as $\chi(T_c) \sim M^2/L^d \sim L^{2-\eta}$, with η being a critical exponent.

We can study the overall fluctuations in the order parameter field for the coating transition $\delta\theta(\mathbf{x}, t) = \theta(\mathbf{x}, t) - \theta$ in the contact line problem. One can define

$$\frac{\Theta^2}{L^d} \equiv \frac{1}{L^d} \int d^d \mathbf{x} d^d \mathbf{x}' \langle \delta\theta(\mathbf{x}, t) \delta\theta(\mathbf{x}', t) \rangle, \quad (36)$$

and use the relation between $\theta(\mathbf{x}, t)$ and $h(\mathbf{x}, t)$ given in Eq. (13), to find

$$\frac{\Theta^2}{L^d} \sim \int d^d \mathbf{x} \int \frac{d^d \mathbf{k}}{(2\pi)^d} k^2 e^{i\mathbf{k}\cdot\mathbf{x}} \langle |h(\mathbf{k}, t)|^2 \rangle, \quad (37)$$

to the leading order. We can now use the scaling form of Eq. (33) in the long time limit, and obtain

$$\frac{\Theta^2}{L^d} \sim \int d^d \mathbf{x} \int \frac{d^d \mathbf{k}}{(2\pi)^d} k^2 e^{i\mathbf{k}\cdot\mathbf{x}} \frac{1}{k^{2\zeta+d}} \sim \int_a^L \frac{dx}{x^{3-d-2\zeta}}, \quad (38)$$

which yields

$$\frac{\Theta^2}{L^d} \sim \begin{cases} 1 & ; \zeta < \frac{2-d}{2} \\ L^{2\zeta+d-2} & ; \zeta > \frac{2-d}{2} \end{cases}. \quad (39)$$

We thus find interestingly that the value of the roughness exponent at the onset of the coating transition can determine the order of the dynamical phase transition: the phase transition is *first order* for $\zeta < \frac{2-d}{2}$, and it is *second order* for $\zeta > \frac{2-d}{2}$. In the case of a second order phase transition, we can define a dynamical exponent

$$\eta = 4 - d - 2\zeta, \quad (40)$$

based on the above analogy with the equilibrium critical phenomena, and an order parameter exponent

$$\beta = (1 - \zeta)\nu, \quad (41)$$

from a naive application of the exponent identities, where ν is the exponent that characterizes the divergence of the correlation length (see below).

Similarly, we can calculate the magnitude of local order parameter fluctuations. We find

$$\langle \delta\theta(\mathbf{x}, t)^2 \rangle \sim \int \frac{d^d \mathbf{k}}{(2\pi)^d} k^2 \langle |h(\mathbf{k}, t)|^2 \rangle, \quad (42)$$

to the leading order, which yields

$$\langle \delta\theta(\mathbf{x}, t)^2 \rangle \sim \int_{\pi/L}^{\pi/a} \frac{dk}{k^{2\zeta-1}} \mathcal{G}(k^z t). \quad (43)$$

and, consequently,

$$\langle \delta\theta(\mathbf{x}, t)^2 \rangle \sim \begin{cases} t^{2(\zeta-1)/z} & ; t \ll L^z \\ \delta\theta_{\text{st}}^2(L) & ; t \gg L^z \end{cases}, \quad (44)$$

where

$$\delta\theta_{\text{st}}(L) \sim \begin{cases} 1 & ; \zeta < 1 \\ \sqrt{\ln(L/a)} & ; \zeta = 1 \\ L^{\zeta-1} & ; \zeta > 1 \end{cases}. \quad (45)$$

The above result shows that the extent of the order parameter fluctuations actually depends on the value of the roughness exponent ζ in the stationary limit, i.e., it will be finite for $\zeta < 1$, and unbounded for $\zeta > 1$. It is important to note that $\zeta > 1$ signals a breakdown of our perturbative scheme in dealing with the nonlinearities in the system, as one can show that the neglected nonlinear terms in Eq. (23) can actually be organized as a power series in the parameter $L^{\zeta-1}$ in the long wavelength limit.

A systematic study of the stochastic dynamics described by Eq. (23) will yield the values of z and ζ , and thus provide us with a characterization of the statistical properties of the moving contact line.

V. CONTACT-ANGLE–VELOCITY RELATION: MEAN-FIELD THEORY FOR THE COATING TRANSITION

The dynamics described in Sec. III, can be first studied in the mean-field approximation, where the contact line is assumed to be a straight line. In this case, the relation between the dynamic contact-angle of the wetting front, and its velocity is given by Eq. (25). It is instructive to examine the limiting behavior of this equation in the two cases of local dissipation and hydrodynamic dissipation scenarios, separately.

A. Local Approach

In this regime, Eq. (25) yields [see also Eq.(B1)]

$$\frac{\theta}{\theta_e} \Big|_l = \sqrt{1 - \frac{2v}{c_{0l}}}, \quad (46)$$

for $v < \frac{c_{0l}}{2}$, while $\theta = 0$ identically for $v > \frac{c_{0l}}{2}$. This function is plotted in Fig. 5.

As can be readily seen from Fig. 5, increasing v would lead to decreasing values of θ until at a critical velocity $v_{cl} = \frac{c_{0l}}{2}$ it finally vanishes continuously. A vanishing contact-angle presumably corresponds to formation of a Landau-Levich film. The value of the dynamic contact-angle θ serves as the order parameter for this dynamical phase transition, while v is the tuning parameter. The continuous vanishing of the order parameter makes the phase transition classified as second order. As in the general theory of critical phenomena, a mean-field exponent $\beta = 1/2$ is characterizing the vanishing of the order parameter in terms of the tuning parameter.

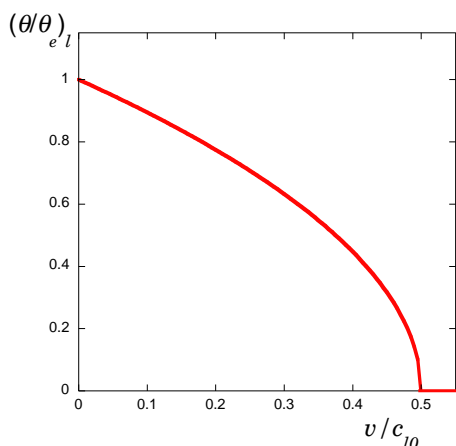


FIG. 5. The reduced order parameter $(\theta/\theta_e)_l$ as a function of the dimensionless velocity v/c_{0l} for local mechanism [Eq. (46)]. The dynamical phase transition at $v_{cl}/c_{0l} = 1/2$ is predicted to be of second order in this picture.

B. Hydrodynamic Approach

In this case, Eq.(25) leads to [see also Eq. (B7)]¹

$$\frac{\theta}{\theta_e} \Big|_h = \frac{1}{\sqrt{3}} \left[\left(-\frac{3\sqrt{3}v}{c_{0h}} - i\sqrt{1 - \frac{27v^2}{c_{0h}^2}} \right)^{1/3} + \left(-\frac{3\sqrt{3}v}{c_{0h}} + i\sqrt{1 - \frac{27v^2}{c_{0h}^2}} \right)^{1/3} \right], \quad (47)$$

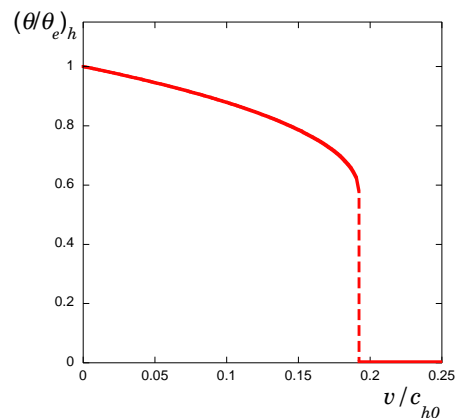


FIG. 6. The reduced order parameter $(\theta/\theta_e)_h$ as a function of the dimensionless velocity v/c_{0h} for the hydrodynamic mechanism [Eq. (47)]. The dynamical phase transition at $v_{ch}/c_{0h} = 1/(3\sqrt{3}) \simeq 0.192$ is predicted to be of first order in this picture.

The above formula, which holds only for $v < \frac{c_{0h}}{3\sqrt{3}}$ has two branches and only the one that recovers $\theta = \theta_e$ for zero velocity is acceptable as plotted in Fig. 6. While at $v = \frac{c_{0h}}{3\sqrt{3}}$ we find $\theta = \frac{\theta_e}{3}$, we expect to have $\theta = 0$ for higher velocities $v > \frac{c_{0h}}{3\sqrt{3}}$. Therefore, the order parameter θ experiences a finite jump at the transition velocity $v_{ch} = \frac{c_{0h}}{3\sqrt{3}}$, which is the hallmark of a first order phase transition.

VI. LINEAR THEORY

One can go beyond the simple mean-field treatment, and study the effect of linear fluctuations on top of the

¹Note that the expression in Eq. (47) is real, and the i is retained only to keep the appearance of the formula simpler.

mean-field theory. There are different aspects to the linear dynamics that one can elaborate on, as considered in this section.

A. Relaxation

We can study the relaxation dynamics of a moving contact line only by using the linear term in Eq. (23). We find that each deformation mode of wavevector k relaxes with a characteristic time scale given as

$$\tau^{-1}(k) = c|k|, \quad (48)$$

where the relaxation velocity c is given as in Eq. (26) above. [See also Eqs. (B2) and (B8) for the limiting forms.]

In fact, one can show from Eqs. (25) and (26), that the relaxation velocity c is related to the slope of the contact-angle-velocity curve as

$$c = -b_0\theta \frac{dv}{d\theta}. \quad (49)$$

This proves that the onset of instability in the contact-angle, signalled by a diverging slope of $d\theta/dv$, exactly corresponds to where the relaxation velocity c vanishes. In other words, exactly at the onset of the coating transition (as found in the mean-field scheme of Sec. V), where the order parameter has a singular behavior, the relaxation becomes infinitely slow, and a distorted the contact line does not relax.

This ‘‘coincidence’’ suggests strongly that the coating transition—the onset of leaving a Landau–Levich film—can be described as a dynamical phase transition in terms of the deformations of the contact line and its statistical roughness on a disordered substrate.

B. Fluctuations

To account for the statistical fluctuations of the moving contact line on a disordered substrate, we can also include the noise term in Eq. (23), and calculate the width of the contact line. We find

$$W(L, t) \sim \begin{cases} \sqrt{t}, & t \ll \frac{a}{c}, \\ \sqrt{\ln \left[\frac{ct}{a} \right]}, & \frac{a}{c} \ll t \ll \frac{L}{c}, \\ \sqrt{\ln \left(\frac{L}{a} \right)}, & t \gg \frac{L}{c}. \end{cases} \quad (50)$$

There are two important time scales in the above equation: (i) the ‘‘microscopic’’ time a/c that corresponds to the crossover from local diffusive dynamics to collective motion along the contact line, and (ii) the ‘‘macroscopic’’ time L/c that corresponds to the crossover to the stationary state. We thus find from Eq. (50) that the stochastic deformations of the contact line are characterized by $\zeta_0 = 0$ and $z_0 = 1$, within the linear theory.

C. Breakdown

The nonlinear term in Eq. (23) will modify the above results if it becomes appreciable at long length scales, as compared to the linear term. To examine under what conditions this may take place, we can estimate the ratio of the two terms in Eq. (23), which scales as

$$\frac{c_0(L/a)^{2\zeta_0-1}}{c(L/a)^{\zeta_0}} \sim \frac{ac_0\sqrt{\ln(L/a)}}{Lc},$$

where c_0 could be set by either c_{0l} or c_{0h} . The nonlinear term is thus appreciable *only* when the smallest time scale in the linear theory a/c becomes comparable to L/c_0 , which happens near the coating transition when c becomes small (see Sec. VI A). This confirms that a consistent study of the coating transition should take a proper account of the nonlinear terms.

VII. EFFECT OF THE NONLINEAR TERM

Let us now attempt to systematically study the dynamical phase transition in the moving contact line using an RG scheme. The dynamical equation, which can be generally written in d dimensions as [33]

$$\partial_t h(\mathbf{k}, t) = -ck h(\mathbf{k}, t) + \eta(\mathbf{k}, t) - \frac{1}{2} \int \frac{d^d \mathbf{q}}{(2\pi)^d} \lambda(\mathbf{q}, \mathbf{k} - \mathbf{q}) h(\mathbf{q}, t) h(\mathbf{k} - \mathbf{q}, t), \quad (51)$$

with $\lambda(\mathbf{q}, \mathbf{k} - \mathbf{q})$ given as in Eq. (24), belongs to the general class of Kardar-Parisi-Zhang (KPZ) equations [34–39]. We take a noise spectrum given by

$$\langle \eta(\mathbf{k}, t) \rangle = 0, \\ \langle \eta(\mathbf{k}, t) \eta(\mathbf{k}', t') \rangle = 2D(2\pi)^d \delta^d(\mathbf{k} + \mathbf{k}') \delta(t - t'), \quad (52)$$

and employ standard RG techniques following Ref. [35] to calculate the RG equations describing the flow of the coupling constants.

A. Perturbation Theory

To perform this calculation, we first need to construct a perturbation theory that takes into account the nonlinear term. This is done more easily if we perform a Fourier transformation in the time variable in Eq. (51), which yields

$$-i\omega h(\mathbf{k}, \omega) = -ck h(\mathbf{k}, \omega) + \eta(\mathbf{k}, \omega) - \frac{1}{2} \int \frac{d\Omega}{2\pi} \frac{d^d \mathbf{q}}{(2\pi)^d} \lambda(\mathbf{q}, \mathbf{k} - \mathbf{q}) \times h(\mathbf{q}, \Omega) h(\mathbf{k} - \mathbf{q}, \omega - \Omega). \quad (53)$$

This equation can then be re-written in the form

$$h(\mathbf{k}, \omega) = G_0(\mathbf{k}, \omega)\eta(\mathbf{k}, \omega) - \frac{1}{2}G_0(\mathbf{k}, \omega) \int \frac{d\Omega}{2\pi} \frac{d^d \mathbf{q}}{(2\pi)^d} \lambda(\mathbf{q}, \mathbf{k} - \mathbf{q}) \times h(\mathbf{q}, \Omega)h(\mathbf{k} - \mathbf{q}, \omega - \Omega), \quad (54)$$

in which the bare response function is given as

$$G_0(\mathbf{k}, \omega) = \frac{1}{ck - i\omega}. \quad (55)$$

We can then define the full response function $G(\mathbf{k}, \omega)$ via

$$h(\mathbf{k}, \omega) = G(\mathbf{k}, \omega)\eta(\mathbf{k}, \omega), \quad (56)$$

and use the spectrum for the Fourier transform of the noise as

$$G^{-1}(\mathbf{k}, \omega) = G_0^{-1}(\mathbf{k}, \omega) - 2D \int_{-\infty}^{\infty} \frac{d\Omega}{2\pi} \int_0^{\Lambda} q^{d-1} dq \frac{S_{d-1}}{(2\pi)^d} \int_0^{\pi} d\theta \sin^{d-2} \theta \times \frac{1}{\left[c\sqrt{q^2 + k^2 - 2kq \cos \theta} - i(\omega - \Omega) \right] (c^2 q^2 + \Omega^2)} \times \left[\lambda_1(q^2 - qk \cos \theta) + \lambda_2 q \sqrt{q^2 + k^2 - 2kq \cos \theta} + \lambda_3 k q + \lambda_3 k \sqrt{q^2 + k^2 - 2kq \cos \theta} - \lambda_3 k^2 \right] \times \left[\lambda_1 k q \cos \theta + \lambda_2 q k + \lambda_3 q \sqrt{q^2 + k^2 - 2kq \cos \theta} + \lambda_3 k \sqrt{q^2 + k^2 - 2kq \cos \theta} - \lambda_3 (q^2 + k^2 - 2kq \cos \theta) \right], \quad (59)$$

where $\Lambda = \pi/a$ is an upper cutoff for the wavevector set by an inverse microscopic length scale, and S_d is the surface area of a unit sphere in d dimensions. We can then perform the frequency integration, expand the integrand in powers of k/q (that is justified because we are interested in the long wavelength behavior of the system), and integrate over the angular variable, to obtain

$$G^{-1}(\mathbf{k}, \omega) = G_0^{-1}(\mathbf{k}, \omega) - \frac{D}{2c^2} \frac{S_d}{(2\pi)^d} \times (\lambda_1 + \lambda_2)(\lambda_2 + \lambda_3) \left(\int q^d dq \right) k. \quad (60)$$

Assuming a same form for the full response function as the bare one, namely

$$G(\mathbf{k}, \omega) = \frac{1}{c_R k - i\omega}, \quad (61)$$

one then obtain a renormalized elastic constant as

$$c_R = c \left\{ 1 - \left[\frac{(\lambda_1 + \lambda_2)(\lambda_2 + \lambda_3)D}{2c^3} \right] \frac{S_d}{(2\pi)^d} \left(\int q^d dq \right) \right\}. \quad (62)$$

A similar calculation can be performed to obtain the renormalized noise amplitude, that is defined via

$$\langle h(\mathbf{k}, \omega)h(-\mathbf{k}, -\omega) \rangle = 2D_R G(\mathbf{k}, \omega)G(-\mathbf{k}, -\omega). \quad (63)$$

one obtains

$$\langle \eta(\mathbf{k}, \omega) \rangle = 0, \quad \langle \eta(\mathbf{k}, \omega)\eta(\mathbf{k}', \omega') \rangle = 2D(2\pi)^{d+1} \delta^d(\mathbf{k} + \mathbf{k}')\delta(\omega + \omega'), \quad (57)$$

to find the response function perturbatively in the λ -parameters.

Up to second order in the perturbation theory, we find

$$G(\mathbf{k}, \omega) = G_0(\mathbf{k}, \omega) + 4 \times \frac{1}{4} G_0(\mathbf{k}, \omega)^2 \times 2D \times \int \frac{d\Omega}{2\pi} \frac{d^d \mathbf{q}}{(2\pi)^d} \lambda(\mathbf{q}, \mathbf{k} - \mathbf{q}) \lambda(-\mathbf{q}, \mathbf{k}) \times G_0(\mathbf{q}, \Omega)G_0(-\mathbf{q}, -\Omega)G_0(\mathbf{k} - \mathbf{q}, \omega - \Omega), \quad (58)$$

which can be re-written as

$$2D_R = 2D + 2 \times \left(\frac{1}{2} \right)^2 \times (2D)^2 \int \frac{d\Omega}{2\pi} \frac{d^d \mathbf{q}}{(2\pi)^d} \times \lambda(\mathbf{q}, \mathbf{k} - \mathbf{q}) \lambda(-\mathbf{q}, \mathbf{q} - \mathbf{k}) G_0(\mathbf{q}, \Omega) G_0(-\mathbf{q}, -\Omega) \times G_0(\mathbf{k} - \mathbf{q}, \omega - \Omega) G_0(\mathbf{q} - \mathbf{k}, \Omega - \omega), \quad (64)$$

which in the small k limit yields

$$D_R = D \left\{ 1 + \left[\frac{(\lambda_1 + \lambda_2)^2 D}{4c^3} \right] \frac{S_d}{(2\pi)^d} \left(\int q^d dq \right) \right\}. \quad (65)$$

Finally, one can show that similar to original KPZ problem [34], none of the λ -parameters are renormalized, so that we have

$$\lambda_R(\mathbf{q}, \mathbf{k} - \mathbf{q}) = \lambda(\mathbf{q}, \mathbf{k} - \mathbf{q}). \quad (66)$$

We can now use the results of the perturbation theory, to construct a perturbative RG scheme.

B. Renormalization Group Calculation

In order to recapitulate the perturbation theory into an RG calculation, we should only integrate out over a layer of wavevectors from Λ/b to Λ and see how the coupling constants are affected by that. This step, which makes up the coarse graining procedure, will lead to the same results as in Eqs. (62), (65), and (66), in which the wavevector integration reads $\int_{\Lambda/b}^{\Lambda} q^d dq =$

$\frac{\Lambda^{d+1}}{d+1} (1 - b^{-(d+1)})$. This should then be followed by the scale transformations $x \rightarrow bx$, $t \rightarrow b^z t$, and $h(x, t) \rightarrow b^S h(x, t)$, which for the scale factor of the form $b = e^l$ and for infinitesimal values of l yields the following RG flow equations for the coupling constant:

$$\begin{aligned} \frac{dc}{dl} &= c[z - 1 - U], \\ \frac{d\lambda(\mathbf{q}, \mathbf{k} - \mathbf{q})}{dl} &= \lambda(\mathbf{q}, \mathbf{k} - \mathbf{q}) (\zeta + z - 2), \\ \frac{dD}{dl} &= D \left[z - 2\zeta - d + \left(\frac{\lambda_1 + \lambda_2}{\lambda_2 + \lambda_3} \right) \frac{U}{2} \right], \end{aligned} \quad (67)$$

in which

$$U = \frac{\pi S_d (\lambda_1 + \lambda_2) (\lambda_2 + \lambda_3) D}{(2a)^{d+1} c^3}. \quad (68)$$

To study the fixed point structure of the above set of flow equations, we set $z = 1 + U$ and $\zeta = 1 - U$, and look at the flow equation for U :

$$\frac{dU}{dl} = -(d+1)U + \left[6 + \left(\frac{\lambda_1 + \lambda_2}{\lambda_2 + \lambda_3} \right) \right] \frac{U^2}{2}, \quad (69)$$

which has two stable fixed points at $U = 0$ (linear theory) and $U = \infty$ (strong coupling), as well as an intermediate unstable fixed point at

$$U = U^* \equiv \frac{2(d+1)}{6 + (\lambda_1 + \lambda_2)/(\lambda_2 + \lambda_3)}. \quad (70)$$

For $U < U^*$, the nonlinearity is irrelevant and the exponents are given by the linear theory, i.e. $\zeta_0 = 0$ and $z_0 = 1$, while for $U > U^*$ the behavior of the system is governed by a strong coupling fixed point which cannot be studied perturbatively. The fixed point at U^* corresponds to a roughening transition of the moving contact line. The exponents at the transition are

$$\begin{aligned} z &= 1 + U^*, \\ \zeta &= 1 - U^*, \end{aligned} \quad (71)$$

which turn out to be nonuniversal. The roughening transition corresponds to the limit of stability of the moving contact line phase. The phase described by the strong

$$\left. \frac{g}{\gamma \theta_e^2} \right|_l = \frac{4 \left(\frac{2b_0^3}{\pi} \right)^{1/2} \left(\frac{\theta}{\theta_e} \right)^3 \left| 1 - \frac{\theta^2}{\theta_e^2} \right|^{1/2}}{\left[1 - (1 - 2b_1 + 2b_2 + 2b_0^2) \frac{\theta^2}{\theta_e^2} \right]^{1/2} \left[1 - (1 - 2b_1 + 14b_2 + 14b_0^2 + 12b_3) \frac{\theta^2}{\theta_e^2} \right]^{1/2}}. \quad (75)$$

Similarly, for the hydrodynamic case, using Eqs. (B7-B12) in Eq. (74) yields an equation for the phase boundary as

$$\left. \frac{g}{\gamma \theta_e^2} \right|_h = \frac{6 \left(\frac{3b_0^3}{\pi} \right)^{1/2} \left(\frac{\theta^2}{\theta_e^2} - \frac{1}{3} \right)^{3/2} \left| 1 - \frac{\theta^2}{\theta_e^2} \right|^{1/2}}{\left[(b_1 - b_2 - 1) + (1 - 3b_1 + 3b_2 + 6b_0^2) \frac{\theta^2}{\theta_e^2} \right]^{1/2} \left[(b_1 - 7b_2 - 6b_3 - 1) + (1 - 3b_1 + 21b_2 + 42b_0^2 + 18b_3) \frac{\theta^2}{\theta_e^2} \right]^{1/2}}, \quad (76)$$

coupling fixed point could presumably correspond to a Landau-Levich film or a pinned contact line.

We can also study how the transition is approached by linearizing the flow equation near the fixed point. Setting $U = U^* + \delta U$, we find $d\delta U/dl = (d+1)\delta U$ that would imply divergence of the correlation length near the transition as

$$\xi \sim |\delta U|^{-\nu}, \quad (72)$$

with

$$\nu = \frac{1}{d+1}. \quad (73)$$

The correlation length corresponds to the typical size of rough segments in the contact line, which should diverge as the transition is approached (See Fig. 1).

VIII. FIXED POINT EQUATION: PHASE DIAGRAM AND EXPONENTS

In principle, the position of a phase boundary that separates the different phases could be obtained from a fixed point equation [such as Eq. (70)]. However, in most RG studies the relation between the phenomenological parameters in the theory and the microscopic parameters are not known, and thus the fixed point equation cannot help us obtain the phase diagram of the system in terms of the real control parameters.

In the present case, however, the fact that we have used some physical models to arrive at the the dynamical equations allows us to make such direct connections. If we use the relations obtained for the parameters as a function of the contact-angle in Sec. III (and Appendix B), and insert them in the fixed point equation Eq. (70) with $d = 1$, which can be written as

$$\frac{D}{a^2} = \frac{8}{\pi} \frac{c^3}{(\lambda_1 + \lambda_2)(\lambda_1 + 7\lambda_2 + 6\lambda_3)}, \quad (74)$$

we can map out the phase diagram of the system, and calculate the value of the exponents.

In the local case, using Eqs. (B1-B6) in Eq. (74) yields an equation for the phase boundary as

These phase boundaries are plotted in Figs. 2 and 3 (solid line) for a choice of parameters $b_0 = 1$, $b_1 = 1$, $b_2 = -1$, and $b_3 = -1$.

The phase boundary that corresponds to a roughening transition of the moving contact line has two different branches. The first branch that happens at relatively high velocities, presumably corresponds to the onset of leaving a Landau–Levich film. In the local case, the phase boundary for this transition start at zero contact-angle for zero disorder, and has a limiting form as reported in Eq. (1) above, with

$$\alpha_{cl} = \frac{(2\pi)^{1/6}}{2\sqrt{b_0}}, \quad (77)$$

whereas in the hydrodynamic case the boundary starts at a finite value of the contact-angle, with the limiting form as reported in Eq. (2), in which

$$\alpha_{ch} = \frac{1}{2\sqrt{3}b_0} \left[\frac{\pi}{6} (3b_0^2 - 1)(21b_0^2 - 1) \right]^{1/3}. \quad (78)$$

We can calculate the value of the exponents along these phase boundaries, and as it turns out they are non-universal. We find

$$\zeta_{cl} = 1 + 2(2\pi)^{1/3} \left(\frac{b_0^2 + b_2 + b_3}{b_0} \right) \left(\frac{g}{\gamma\theta_e^2} \right)^{2/3}, \quad (79)$$

$$z_{cl} = 1 - 2(2\pi)^{1/3} \left(\frac{b_0^2 + b_2 + b_3}{b_0} \right) \left(\frac{g}{\gamma\theta_e^2} \right)^{2/3}, \quad (80)$$

for the local case, and

$$\zeta_{ch} = \frac{3 - 1/(3b_0^2)}{7 - 1/(3b_0^2)} - \frac{(36\pi)^{1/3}}{b_0} \frac{(3b_0^2 - 1)^{1/3}}{(21b_0^2 - 1)^{5/3}} [3b_0^2(b_1 + b_3 - 1) - b_2 - b_3] \left(\frac{g}{\gamma\theta_e^2} \right)^{2/3}, \quad (81)$$

$$z_{ch} = \frac{11 - 1/(3b_0^2)}{7 - 1/(3b_0^2)} + \frac{(36\pi)^{1/3}}{b_0} \frac{(3b_0^2 - 1)^{1/3}}{(21b_0^2 - 1)^{5/3}} [3b_0^2(b_1 + b_3 - 1) - b_2 - b_3] \left(\frac{g}{\gamma\theta_e^2} \right)^{2/3}, \quad (82)$$

for the hydrodynamic case.

The other branch of the phase boundaries appear very near the equilibrium contact-angle corresponding to low velocities, and presumably corresponds to the onset of pinning. In other words, the pinning transition (as opposed to the depinning transition) can be described as a roughening of the contact line imposed by the static minimum energy configuration on the disordered substrate, as it slows down to rest. The shape of the phase boundaries for weak disorder can be found for the local case as in Eq. (3) above, with

$$\alpha_{pl} = \frac{3\pi}{4b_0^3} (b_0^2 + b_2 - b_1)^2 \left[\frac{1}{6} + \left(\frac{b_0^2 + b_2 + b_3}{b_0^2 + b_2 - b_1} \right) \right], \quad (83)$$

and, for the hydrodynamic case as in Eq. (4) above, with

$$\alpha_{ph} = \frac{3\pi}{4b_0^3} (3b_0^2 + b_2 - b_1)^2 \left[\frac{1}{6} + \left(\frac{3b_0^2 + b_2 + b_3}{3b_0^2 + b_2 - b_1} \right) \right]. \quad (84)$$

The above prediction for the phase boundary of the pinning transition is in agreement with a previous prediction based on the hysteresis in receding and advancing

contact-angles [16]. We can calculate the corresponding exponents along the depinning transition phase boundary, and find

$$\zeta_{pl} = \frac{1 + \frac{1}{2} \left(\frac{b_0^2 + b_2 - b_1}{b_0^2 + b_2 + b_3} \right)}{3 + \frac{1}{2} \left(\frac{b_0^2 + b_2 - b_1}{b_0^2 + b_2 + b_3} \right)}, \quad (85)$$

$$z_{pl} = \frac{5 + \frac{1}{2} \left(\frac{b_0^2 + b_2 - b_1}{b_0^2 + b_2 + b_3} \right)}{3 + \frac{1}{2} \left(\frac{b_0^2 + b_2 - b_1}{b_0^2 + b_2 + b_3} \right)}, \quad (86)$$

for the local case, and

$$\zeta_{ph} = \frac{1 + \frac{1}{2} \left(\frac{3b_0^2 + b_2 - b_1}{3b_0^2 + b_2 + b_3} \right)}{3 + \frac{1}{2} \left(\frac{3b_0^2 + b_2 - b_1}{3b_0^2 + b_2 + b_3} \right)}, \quad (87)$$

$$z_{ph} = \frac{5 + \frac{1}{2} \left(\frac{3b_0^2 + b_2 - b_1}{3b_0^2 + b_2 + b_3} \right)}{3 + \frac{1}{2} \left(\frac{3b_0^2 + b_2 - b_1}{3b_0^2 + b_2 + b_3} \right)}, \quad (88)$$

for the hydrodynamic case.

The two branches of the phase boundaries meet at a junction point, called T in Figs. 2 and 3, where they both develop a vanishing slope as obtained from Eqs. (75) and (76).

Although the fact that we do not know the values of the numerical constants b_n makes us unable to predict the values of the exponents, we can nevertheless put some bounds on them using simple physical requirements. For example, we expect on physical grounds that the critical contact-angle for the coating transition increases with disorder. Then Eqs. (2) and (78), together with a requirement that we have a roughness exponent that is less than one, imply that $b_0^2 > 1/3$, which results in a criterion

$$\frac{1}{3} < \zeta_{ch} < \frac{3}{7}, \quad (89)$$

for the roughness exponent in the hydrodynamic case. In the local case, to have a roughness exponent that is less than one we should have $b_0^2 + b_2 + b_3 < 0$, as can be seen from Eq. (79).

From the above results and bounds on the values of the roughness exponents in the two different approaches, and the analysis of Sec. IV, we can conclude that at least in the weak disorder limit $\zeta_{cl} > \frac{1}{2}$ and $\zeta_{ch} < \frac{1}{2}$, and thus the coating transition remains to be first order in the hydrodynamic picture and second order in the local picture even beyond mean-field theory, i.e. within the RG scheme.

On the pinning transition boundary a similar requirement that the advancing (receding) contact-angle increases (decreases) with disorder (together with a requirement that we have a roughness exponent that is less than one) leads to $\left(\frac{b_0^2 + b_2 - b_1}{b_0^2 + b_2 + b_3}\right) > 0$, as can be seen from Eqs. (3) and (83), which implies

$$\zeta_{pl} > \frac{1}{3}, \quad (90)$$

and $\left(\frac{3b_0^2 + b_2 - b_1}{3b_0^2 + b_2 + b_3}\right) > 0$, as can be seen from Eqs. (4) and (84), which implies

$$\zeta_{ph} > \frac{1}{3}. \quad (91)$$

The above results are in agreement with the experimentally observed roughness exponent of about 0.5 for both liquid Helium on a Cesium substrate [25] and water on glass experiments [26].

IX. DISCUSSION

The above study of the dynamics of a moving contact line on a disordered substrate reveals that both the instability corresponding to the onset of leaving a Landau–Levich film at high velocities, and the pinning of the

contact line to the substrate at low velocities, can be described in a unified framework as roughening transitions in the contact line. For advancing contact lines, the phase boundary corresponding to pinning extends continuously to the strong disorder regime. For the receding case, however, the phase boundaries corresponding to pinning and to Landau–Levich transition asymptote to a maximum with zero slope, where we identify as a junction point, denoted by T in Figs. 2 and 3.

For stronger disorder, the pinned contact line presumably goes directly into the Landau–Levich phase: the edge of the liquid drop is pinned so strongly that it remains still when the liquid wedge starts to move upon decreasing the contact-angle, and thus a film is left behind. In this sense, at the dashed line in the phase diagram (Figs. 2 and 3) nothing really happens to the contact line itself, while the body of the liquid drop is “depinned.” This behavior has in fact been observed in experiments with liquid Helium on a Cesium substrate, where the receding contact-angle has always been found to vanish identically immediately after depinning [18,25]. It is also interesting to note that a non-universality of the roughness exponent at the depinning threshold, manifesting itself in the form of a dependence on the value of the contact-angle, has also been reported in Ref. [25].

One can get a plausible picture of the roughening transition in terms of fluctuating domains of different sizes, in analogy with equilibrium phase separations in, say, binary mixtures. As it is sketched in Fig. 1, a portion of the moving contact line can be instantaneously pinned to a defect on the substrate, thereby nucleating a domain where the liquid is pinned to the substrate. These domains are rough, because the contact line has to conform to the minimal energy configuration imposed by the substrate disorder, and they can exist in length scales up to the correlation length ξ . As the transition is approached, the correlation length increases until at some point one of the domains enlarge to a macroscopic scale and span the whole system, corresponding to the divergence of the correlation length at the critical point. Interestingly, the same picture can be attributed to both the coating transition and the pinning transition. The difference comes from the fact that in the pinning transition the substrate can stop both the contact line and the liquid from motion, while in the coating transition where the liquid is already moving at relatively high velocities it can only stop the contact line and not the liquid, as mentioned above.

One can use a scaling argument to account for the power law in Eqs. (1) and (2). If we take the above KPZ equation and make the scale transformations $t \rightarrow ct$, and $h \rightarrow \sqrt{D}/ch$, the coefficient of the linear term as well as the strength of the noise term will be set to one, and the only remaining coupling constant (the coefficient of the nonlinear term) will have the form $\lambda D^{1/2}/c^{3/2}$. We expect the roughening transition to take place when this coupling constant is of order unity, which yields

Eqs. (1) and (1) when the values $D \sim g^2$, $c_l \sim \frac{\theta_c^2}{\theta_e^2}$, $c_h \sim \left(\frac{\theta_c}{\theta_e} - \frac{1}{\sqrt{3}}\right)$, and $\lambda \sim \text{const.}$ are used.

In treating the disorder contribution, we have made the assumption that the dependence in the noise term η on the shape of the contact line can be neglected for any non-vanishing drift velocity. While this approximation can be supported by a naive power counting, it may be argued that more a sophisticated functional RG approach is necessary to deal with this dependence [21,23], since upon approaching the pinning transition the contact line velocity becomes progressively small. In this sense, the exact values of the exponents derived for the pinning transition boundary, which are non-universal anyway, and the predictions about the nature of the junction point may not be trusted. However, we do believe that the main features of the above results—the non-universality of the exponents, the existence of the junction point, and the form of the pinning phase boundary, will persist.

We finally mention that this work can hopefully motivate two types of experiments. One can try to probe the relaxation of a moving contact line, similar to the

Ondarcuhu–Veyssie experiment on a static contact line [12], and measure the velocity dependence of the dispersion relation. This dependence could be used to determine the dominant dissipation mechanism [28]. It is also interesting to systematically study the coating transition (onset of leaving a Landau–Levich film) for receding contact lines on a disordered substrate using video microscopy techniques. In particular, it would be interesting to look for a roughening of the contact line before the Landau–Levich film is formed, and measure the corresponding roughness exponents.

ACKNOWLEDGMENTS

We are grateful to A. Ajdari, J. Bico, R. Bruinsma, P.G. de Gennes, C. Guthmann, M. Kardar, W. Krauth, L. Limat, S. Moulinet, D. Quéré, E. Rolley, A. Rosso, and H. Stone for valuable discussions and comments. One of us (R.G.) would like to thank the group of Prof. de Gennes at College de France for their hospitality and support during his visit.

APPENDIX A: GEOMETRY OF THE SURFACE NEAR THE CONTACT LINE

Here we briefly review some of the aspects of the differential geometry of surfaces that are useful in this context. The free surface of the liquid can be described by the embedding

$$\mathbf{R}(x, y) = (x, y, z(x, y)), \quad (\text{A1})$$

using which we can find two independent unit tangent vectors to the surface at each point

$$\hat{\mathbf{t}}_x \equiv \frac{\partial_x \mathbf{R}}{|\partial_x \mathbf{R}|} = \frac{1}{\sqrt{1 + (\partial_x z)^2}}(1, 0, \partial_x z), \quad (\text{A2})$$

and

$$\hat{\mathbf{t}}_y \equiv \frac{\partial_y \mathbf{R}}{|\partial_y \mathbf{R}|} = \frac{1}{\sqrt{1 + (\partial_y z)^2}}(0, 1, \partial_y z). \quad (\text{A3})$$

We can also define the unit tangent vector for the contact line (see Fig. 4) as

$$\hat{\mathbf{t}} = \frac{1}{\sqrt{1 + (\partial_x h)^2}}(1, \partial_x h, 0). \quad (\text{A4})$$

To find the unit vector $\hat{\mathbf{T}}$, that shows the local direction at which the surface tension force is acting (see Fig. 4), we should note that it is tangent to the surface, so it can be written as

$$\hat{\mathbf{T}} = u_x \hat{\mathbf{t}}_x + u_y \hat{\mathbf{t}}_y. \quad (\text{A5})$$

Imposing the requirements that it is perpendicular to the contact line $\hat{\mathbf{T}} \cdot \hat{\mathbf{t}} = 0$ and that it is a unit vector $\hat{\mathbf{T}}^2 = 1$, yields the two parameters, and we obtain

$$\hat{\mathbf{T}} = \frac{(-\partial_x h, 1, -\partial_x h \partial_x z + \partial_y z)}{\{1 + (\partial_y z)^2 + (\partial_x h)^2 [1 + (\partial_x z)^2] - 2(\partial_x h)(\partial_x z)(\partial_y z)\}^{1/2}}. \quad (\text{A6})$$

We can also define the unit vector normal to the contact line (see Fig. 4) as

$$\hat{\mathbf{n}} = \frac{1}{\sqrt{1 + (\partial_x h)^2}}(-\partial_x h, 1, 0), \quad (\text{A7})$$

using which we can define the local contact-angle as

$$\theta(x) = \cos^{-1}(\hat{\mathbf{T}} \cdot \hat{\mathbf{n}}), \quad (\text{A8})$$

where

$$\hat{\mathbf{T}} \cdot \hat{\mathbf{n}} = \frac{\sqrt{1 + (\partial_x h)^2}}{\{1 + (\partial_y z)^2 + (\partial_x h)^2 [1 + (\partial_x z)^2] - 2(\partial_x h)(\partial_x z)(\partial_y z)\}^{1/2}}. \quad (\text{A9})$$

Note that we have $\sqrt{1 + (\partial_x h)^2} \hat{\mathbf{T}} \cdot \hat{\mathbf{y}} = \cos \theta(x)$.

APPENDIX B: COUPLING CONSTANTS IN THE TWO DIFFERENT APPROACHES

In this Appendix, we have summarized the limiting form of the coupling constants of the dynamical equation, corresponding to each of the dissipation mechanisms separately.

1. Local Approach

The asymptotic form of the equations given in Sec. III can be obtained in this case by taking the limit $c_{0h}/c_{0l} \rightarrow \infty$. One obtains

$$v|_l = \frac{c_{0l}}{2} \left(1 - \frac{\theta^2}{\theta_e^2}\right), \quad (\text{B1})$$

for the contact-angle–velocity relation,

$$c_l = b_0 c_{0l} \frac{\theta^2}{\theta_e^2}, \quad (\text{B2})$$

for the relaxation speed, and

$$\lambda_{1l} = \frac{c_{0l}}{2} \left[(1 - 2b_1) \frac{\theta^2}{\theta_e^2} - 1 \right], \quad (\text{B3})$$

and

$$\lambda_{2l} = (b_2 + b_0^2) c_{0l} \frac{\theta^2}{\theta_e^2}, \quad (\text{B4})$$

and

$$\lambda_{3l} = b_3 c_{0l} \frac{\theta^2}{\theta_e^2}, \quad (\text{B5})$$

for the nonlinear coupling constants. We can also find the strength of the noise term as

$$D_l = \frac{a^2 c_{0l}}{\left|1 - \frac{\theta^2}{\theta_e^2}\right|} \left(\frac{g}{\gamma \theta_e^2}\right)^2. \quad (\text{B6})$$

2. Hydrodynamic Approach

The corresponding asymptotic forms of the equations given in Sec. III in this case can be obtained by taking the limit $c_{0h}/c_{0l} \rightarrow 0$. One obtains

$$v|_h = \frac{c_{0h}}{2} \frac{\theta}{\theta_e} \left(1 - \frac{\theta^2}{\theta_e^2}\right), \quad (\text{B7})$$

for the contact-angle–velocity relation,

$$c_h = b_0 \frac{c_{0h}}{2} \frac{\theta}{\theta_e} \left(3 \frac{\theta^2}{\theta_e^2} - 1\right), \quad (\text{B8})$$

for the relaxation speed, and

$$\lambda_{1h} = \frac{c_{0h}}{2} \frac{\theta}{\theta_e} \left[(b_1 - 1) + (1 - 3b_1) \frac{\theta^2}{\theta_e^2} \right], \quad (\text{B9})$$

and

$$\lambda_{2h} = \frac{c_{0h}}{2} \frac{\theta}{\theta_e} \left[-b_2 + (3b_2 + 6b_0^2) \frac{\theta^2}{\theta_e^2} \right], \quad (\text{B10})$$

and

$$\lambda_{3h} = b_3 \frac{c_{0h}}{2} \frac{\theta}{\theta_e} \left(3 \frac{\theta^2}{\theta_e^2} - 1\right), \quad (\text{B11})$$

for the nonlinear coupling constants. We can also find the strength of the noise term as

$$D_h = \frac{a^2 c_{0h}}{\left|1 - \frac{\theta^2}{\theta_e^2}\right|} \left(\frac{\theta}{\theta_e}\right) \left(\frac{g}{\gamma \theta_e^2}\right)^2. \quad (\text{B12})$$

[1] P.G. de Gennes, Rev. Mod. Phys. **57**, 827 (1985).

- [2] T.D. Blake and J.M. Haynes, *J. Colloid Interface Sci.* **30**, 421 (1969); T. Blake in *AIChE International Symposium on the mechanics of thin film coating* (New Orleans, 1988).
- [3] T.D. Blake and K.J. Ruschak, *Nature* **282**, 489 (1979).
- [4] See also: O.V. Voinov, *Fluid Dyn. Engl. Transl.* **11**, 714 (1976).
- [5] R.G. Cox, *J. Fluid Mech.* **168**, 169 (1986).
- [6] P.G. de Gennes, *Colloid & Polymer Sci.* **264**, 463 (1986).
- [7] P.G. de Gennes, in *Physics of Amphiphilic Layers* eds. J. Meunier, D. Langevin, and N. Boccardo (Springer, Berlin, 1987); F. Brochard-Wyart, J.M. di Meglio, and D. Quéré, *C. R. Acad. Sci. (Paris)* **304 II**, 553 (1987).
- [8] L. Landau and B. Levich, *Acta Physicochim. USSR* **17**, 42 (1942).
- [9] B. Levich, *Physicochemical Hydrodynamics* (Prentice-Hall, London, 1962).
- [10] J.F. Joanny and P.G. de Gennes, *J. Chem. Phys.* **81**, 552 (1984); Y. Pomeau and J. Vannimenus, *J. Colloid Interface Sci.* **104**, 477 (1985).
- [11] P.G. de Gennes, *C. R. Acad. Sc. Paris II* **302**, 731 (1986).
- [12] T. Ondarcuhu and M. Veyssie, *Nature* **352**, 418 (1991).
- [13] J.-M. di Meglio, *Europhys. Lett.* **17**, 607 (1992).
- [14] A. Paterson and M. Fermigier, *Phys. Fluids* **9**, 2210 (1997).
- [15] D. Huse, unpublished (cited in Ref. [1]).
- [16] M.O. Robbins and J.F. Joanny, *Europhys. Lett.* **3**, 729 (1987).
- [17] A. Hazareesing and M. Mezard, *Phys. Rev. E* **60**, 1269 (1999).
- [18] C. Guthmann, R. Gombrowicz, V. Repain, and E. Rolley, *Phys. Rev. Lett.* **80**, 2865 (1998).
- [19] E. Raphaël and P.G. de Gennes, *J. Chem. Phys.* **90**, 7577 (1989);
- [20] J.F. Joanny and M.O. Robbins, *J. Chem. Phys.* **92**, 3206 (1990).
- [21] D. Ertas and M. Kardar, *Phys. Rev. E* **49**, R2532 (1994).
- [22] E. Schäffer and P. Wong, *Phys. Rev. Lett.* **80**, 3069 (1998); *Phys. Rev. E* **61**, 5257 (2000).
- [23] P. Chauve, P. Le Doussal, and K.J. Wiese, *Phys. Rev. Lett.* **86**, 1785 (2001).
- [24] A. Rosso and W. Krauth, preprint cond-mat/0107527.
- [25] A. Prevost, E. Rolley, and C. Guthmann, *Phys. Rev. B* **65**, 064517 (2002).
- [26] S. Moulinet, C. Guthmann, and E. Rolley, *Eur. Phys. J. B*, submitted (2002).
- [27] R. Golestanian and E. Raphaël, *Europhys. Lett.* **55**, 228 (2001); Erratum, *Europhys. Lett.* **57**, 304 (2002).
- [28] R. Golestanian and E. Raphaël, *Phys. Rev. E* **64**, 031601 (2001).
- [29] C. Huh and L. Scriven, *J. Colloid Interface Sci.* **35**, 85 (1971).
- [30] Note that from geometry (see Appendix A) we have $\sqrt{1 + (\partial_x h)^2} \hat{\mathbf{T}} \cdot \hat{\mathbf{y}} = \cos \theta(x, t)$.
- [31] F. Brochard-Wyart and P.G. de Gennes, *Adv. Colloid Interface Sci.* **39**, 1 (1992).
- [32] For some recent works related to this problem, see for example: P.G. de Gennes, X. Hua, and P. Levinson, *J. Fluid Mech.* **212**, 55 (1990); J.A. Diez, L. Kondie, and A. Bertozzi, *Phys. Rev. E* **63**, 011208 (2000); H.A. Stone, L. Limat, S.K. Wilson, J.-M. Flesselles, and T. Podgorski, *C. R. Physique* **3**, 103 (2002); J. King and M. Bowen, preprint (2002).
- [33] Note that in this section, we are dealing with d -dimensional wavevectors, and we are using the notation $k = |\mathbf{k}|$ for simplicity. This is to be contrasted from previous sections where k stands for a one dimensional vector taking both positive and negative values.
- [34] M. Kardar, G. Parisi, and Y.-C. Zhang, *Phys. Rev. Lett.* **56**, 889 (1986).
- [35] E. Medina, T. Hwa, M. Kardar, and Y.C. Zhang, *Phys. Rev. A* **39**, 3053 (1989).
- [36] T. Halpin-Healy and Y.-C. Zhang, *Phys. Rep.* **254**, 215 (1995).
- [37] E. Frey and U.C. Täuber, *Phys. Rev. E* **50**, 1024 (1994); *Phys. Rev. E* **51**, 6319 (1995).
- [38] K.J. Wiese, *Phys. Rev. E* **56**, 5013 (1997).
- [39] For a somewhat related study of a non-analytical KPZ equation for interface flow in random media, see: V. Ganesan and H. Brenner, *Phys. Rev. Lett.* **81**, 578 (1998).